Correlation of magnetotransport and structure in sputtered Co/Cu multilayers

2003 J. Phys.: Condens. Matter 15 2471

(http://iopscience.iop.org/0953-8984/15/17/304)

INSTITUTE OF PHYSICS PUBLISHING JOURNAL OF PHYSICS: CONDENSED MATTER

J. Phys.: Condens. Matter **15** (2003) 2471–2491 PII: S0953-8984(03)59376-6

Correlation of magnetotransport and structure in sputtered Co/Cu multilayers

Amitesh Paul[1], **Thorsten Damm, Daniel E Bürgler, Simon Stein, Hermann Kohlstedt and Peter Grünberg**

Institut für Festkörperforschung, Forschungszentrum Jülich GmbH, D-52425 Jülich, Germany

E-mail: A.Paul@fz-juelich.de

Received 10 February 2003
Published 22 April 2003
Online at stacks.iop.org/JPhysCM/15/2471

Abstract

Magnetic multilayer structures of Co/Cu prepared by dc magnetron sputtering are studied with respect to changing number of bilayers (N) for different thicknesses of the Cu spacer layer corresponding to different coupling conditions according to the oscillatory interlayer exchange coupling. X-ray reflectivity and diffuse scattering show that the multilayers become smoother with increasing N. The growth exponent of the roughness is found to be lower for a multilayer than for a single-layer film of similar thickness. The roughness of subsequent interfaces along the stack is conformal, and the lateral correlation does not change with the period number, but depends on the thickness of the spacer layers. The improved layer structure for larger N increases the antiferromagnetic coupling fraction as inferred from magneto-optic Kerr effect measurements and thereby increases the giant magnetoresistance (GMR) ratio up to 35% for $N = 10$. Thus, the first few bilayers do not contribute to the GMR but act as a buffer to improve the growth conditions for the following bilayers. The first about five bilayers can be replaced by a bottom Co layer of equivalent thickness which also improves the layer structure for a subsequently deposited lower number of bilayers without much loss in the GMR ratio. This smoothening effect due to the increasing of the thickness of the bottom-most layer is related to the simultaneously decreasing grain size.

1. Introduction

Ferromagnetic layers separated by non-magnetic spacers have been extensively investigated in the last decade mainly due to the giant magnetoresistance (GMR) properties and the oscillatory interlayer exchange coupling between two adjacent magnetic films [1–4]. The oscillation from ferromagnetic (FM) to antiferromagnetic (AF) coupling between the magnetic layers is

[1] Author to whom any correspondence should be addressed.

0953-8984/03/172471+21$30.00

dependent on the thickness of the spacer layer. When the spacer is of a thickness yielding AF coupled magnetic layers, a change in magnetic configuration is caused by an external saturating (or switching) field which aligns the magnetizations of adjacent magnetic layers parallel. The associated drop in electrical resistivity due to the change in magnetic configuration from antiparallel to parallel is termed GMR.

These physical properties are closely related to the structure of the multilayers (MLs). In particular, the interface roughness has always been in the focus of investigations as it is an important property determining the quality of an ML from the scientific as well as practical perspective. Although the role of interfaces for the magnetic properties has been extensively studied [5, 6], the evolution of the roughness along the ML stack or the effect of the ML growth mechanism on the roughness have hardly been addressed [7]. In general, the evolution of the roughness depends on the lateral wavelength of the roughness (i.e. the lateral correlation length), the thermodynamic properties of the constituent layers and the kinetic properties of the deposited atoms. Considerable experimental and theoretical effort has been put on the understanding the kinetic and thermodynamic factors that control the growth of thin film and ML [8–10]. However, various deposition methods and deposition conditions do not necessarily result in the same growth mechanism. Moreover, although a number of studies have been done by various investigators on non-magnetic MLs of Nb/Si [8], W/Si [11], Pt/C [12] or W/C [13], hardly any study on the scaling behaviour of interface morphology has been reported for magnetic MLs. In the present work only the thickness of the individual layers and the number of bilayers in magnetic MLs are varied in order to understand the influence of interfacial features on the overall ML performance. Our results are particularly interesting not only from the thin film growth point of view but also from that of magnetic MLs, as they show the importance of understanding the physics of ML growth and its influence on the magnetic and magnetotransport properties.

Co/Cu systems have attracted much interest due to their high GMR amplitude of up to $\approx$80% at room temperature (RT) in sputtered, polycrystalline MLs [14–16]. Large GMR ratios and high field sensitivity observed at the first two AF coupling maxima at Cu thicknesses $t_{\mathrm{Cu}} \approx 0.9$ and 2.0 nm make Co/Cu ML attractive for the use in sensor devices [17, 18]. In previous reports of high GMR ratios in ML systems with the current in the plane of the layers (CIP geometry), the number of bilayers (N) was kept large ($N > 50$), and a sufficiently large N was supposed to play an important role for high GMR ratios [14, 15]. The observed enhancement of the GMR ratio with N was mainly attributed to enhanced interfacial, spin-dependent scattering. However, the interfacial scattering contribution to GMR depends on the interface structure of all interfaces in the ML and is thus related to the ML growth. Each growth mechanism yields certain interface roughnesses and an evolution along the whole stack of the ML. An increase of N may influence structural parameters such as the rms (root-mean-square) correlated and uncorrelated interface roughness as well as the roughness correlation lengths in lateral (in the plane of the layers) and vertical (perpendicular to the plane of the layers) directions [7]. These parameters in turn affect the magnetic and magnetotransport properties of a magnetic ML [19]. Therefore, the development of the interface structure is an important property of a structure.

The interface structure development is in general a function of the method of deposition and the deposition conditions. Additionally, the roughness depends on (i) the number of bilayers N, (ii) the thickness $\Lambda = d_A + d_B$ of an A/B bilayer and (iii) the ratio Γ defined as d_A/Λ, where d_A and d_B are the thicknesses of the individual layers A and B, respectively. Generally, the evolution of roughness is quite different in the case of a single-layer thin film and that of an ML of the same total thickness. This is mainly due to the influence of the interfaces in an ML, which introduce for instance lattice mismatch and variations of the surface

energy during growth. Thus, the effect of increasing N while keeping the individual layer thicknesses d_A and d_B constant is quite different from the effect of increasing individual layer thicknesses. In an earlier study by Fullerton *et al* [8] it was found that for non-magnetic Nb/Si MLs grown by magnetron sputtering at high sputter gas pressure there is a dramatic change in roughness when N increases. Recently, Freitag and Clemens [20] reported an increase of lateral correlation lengths with increasing N or increasing Γ in Si/Mo MLs. On the other hand, Paul and Lodha [12] found no significant change in the lateral or vertical correlation lengths for Pt/C ML when only Γ was changed. Although samples were deposited by magnetron sputtering in all three cases [8, 12, 20], the results are quite different and depend on the parameters varied and even on the system chosen. Thus, general predictions are not possible.

In magnetic MLs, variations of Γ or Λ are not suited to study the effect of interface evolution on magnetotransport since each change of the non-magnetic spacer thickness strongly modifies the magnetic interlayer coupling, which in its turn influences magnetotransport. Thus, the effect can best be studied by varying N while keeping Γ constant. To the best of our knowledge there are no experimental studies that connect the evolution of structural parameters and magnetotransport for Co/Cu MLs. The works of various groups on structural investigation of the Co/Cu system such as Ueda *et al* [21] and Saito *et al* [22] were on structures modified by changing the deposition conditions or thermal annealing and thus do not necessarily bring out the effect of structure evolution. Lucinski *et al* [23] have recently measured GMR and hysteresis loops *in situ* during the deposition of Co/Cu MLs. They found changes of the GMR ratio and the hysteresis loops during the growth of the MLs, but the evolution of the structure was not monitored. The low GMR ratio ($\approx$1.7% at the second maximum of the AF coupling) indicates non-optimized structural properties.

Here, we directly address the change in the structural parameters of the ML and their influence on the AF interlayer coupling and on the GMR effect as N increases. To do so, we study (i) the dependence of the microstructure of the ML on N and (ii) its influence on the AF coupling as well as on the GMR ratio and (iii) compare the results for the first and second AF coupling maxima. The aim is to develop an understanding concerning (i) the morphological development of interfaces for increasing N and (ii) the interplay between morphology and AF coupling on one hand and GMR on the other hand. This understanding is expected to be helpful for optimizing ML structures for GMR applications.

2. Experimental details

The MLs studied in the present work are structures of Co/Cu prepared by dc magnetron sputtering. Our deposition system is equipped with eight sputtering targets, and a base pressure of 1×10^{-7} mbar is achieved by turbo-molecular pumps. Samples are prepared by alternate deposition of Co and Cu layers on SiO_2 substrates kept at RT. The sputtering pressure of 3.4×10^{-3} mbar is controlled by the flow of 99.9999% pure Ar in the chamber. The sputtering rates are kept at 0.06 and 0.04 nm s^{-1} for Co and Cu, respectively. The substrate holder is rotated to achieve good deposition homogeneity.

Four different series of MLs labelled S1, S2, S3 and S4 with structures as indicated in table 1 are studied. Series S1, S2 and S3 differ by the Cu spacer thickness: 1.02 nm for series S1 corresponds to the first AF coupling maximum and 2.20 nm for series S2 to the second AF maximum of the oscillatory interlayer coupling across Cu. For series S3 the Cu thickness is 2.5 nm yielding minimal AF coupling. In these three series the number of bilayers N is varied. In series S4, finally, the thickness of the bottom-most Co layer is varied while the number of bilayers is is kept constant ($N = 5$).

Table 1. Structures of the four ML series. N is the number of bilayers and t_{Co} the thickness of the bottom-most Co layer. S1 and S2 correspond to Cu thicknesses around the first and second AF maxima of the oscillatory interlayer coupling, respectively. S3 denotes a Cu thickness yielding weak AF coupling just beyond the second AF maximum. The thickness of the bottom-most Co layer t_{Co} is varied in series S4.

Series	Structure	Variation in series
S1	SiO_2/Co(1.45 nm)/[Cu(1.02 nm)/Co(1.45 nm)]$_{\times N}$	$N = 3$, 5, 6, 8, 10, 20 and 40
S2	SiO_2/Co(1.45 nm)/[Cu(2.20 nm)/Co(1.45 nm)]$_{\times N}$	$N = 3$, 5, 10 and 20
S3	SiO_2/Co(1.45 nm)/[Cu(2.50 nm)/Co(1.45 nm)]$_{\times N}$	$N = 5$, 10, 15 and 20
S4	SiO_2/Co(t_{Co})/[Cu(1.02 nm)/Co(1.45 nm)]$_{\times 5}$	$t_{Co} = 1.45$, 1.68, 1.95, 2.10, 2.25, 2.45, 6.15 and 15.1 $\pm$ 0.05 nm

The microstructure and the layer quality are investigated by low angle x-ray reflectivity (XRR) and x-ray diffuse scattering (XDS) measurements [10, 12, 24]. XRR and XDS measurements are done using a Bruker-axs D8 diffractometer with Cu Kα radiation equipped with Göbel mirrors for the incident and reflected beams instead of conventional Soller slits. These parabolic mirrors provide a directional selection of the beam instead of the positional one of Soller slits. With the source and the detector being in the focus of the parabola, the mirrors not only monochromatize the beam by Bragg reflection and thus suppress the Kβ radiation, but also reject the fluorescent light on the detector side. This set-up results in a gain of intensity by one order of magnitude, which is very helpful for extracting details of the structural characteristics of MLs. Figure 1(a) shows the set-up for the x-ray experiments. We measured in specular geometry with the angle of incidence θ_i equal to the exit angle θ_f as well as in off-specular geometry with an offset of $\Delta\omega = 0.13^\circ$ between θ_i and θ_f. Rocking curve measurements show that at an offset of 0.1° the specularly reflected component is almost completely removed. Thus, in a scan with offset $\Delta\omega = 0.13^\circ$ one measures the diffuse scattering as a function of the component of the momentum transfer vector normal to the sample plane, q_z. True specular reflectivity is obtained by subtracting the off-specularly reflected intensity from the specular one. Diffuse scattering as a function of the in-plane component of the momentum transfer vector, q_x, is measured by keeping the scattering angle 2θ fixed and rocking the specimen around $\theta_i = \theta_f$.

The surface topography of a complete ML is characterized *ex situ* by atomic force microscope (AFM) measurements in tapping mode using a multimode SPM from Digital Instruments.

Magnetoresistance is measured by the conventional four-probe dc technique. Hysteresis loops are recorded by the magneto-optic Kerr effect (MOKE) and also with a superconducting quantum interference device (SQUID) magnetometer. The magnetic field is always applied in the plane of the sample and along a magnetic easy axis. All measurements are performed at RT.

3. Variation of the number of bilayers

3.1. Structural characterization

In specular reflectivity measurements, the momentum transfer is perpendicular to the sample surface, $q = q_z$. This type of measurement provides information about the individual layer thicknesses and an estimate of the rms interfacial roughness.

However, scattering of electromagnetic radiation from non-ideal surfaces and interfaces results in a loss of specular reflectivity and gives rise to non-specular reflectivity. The incoherent (diffuse) component of the scattered intensity depends on in-plane components of the scattering

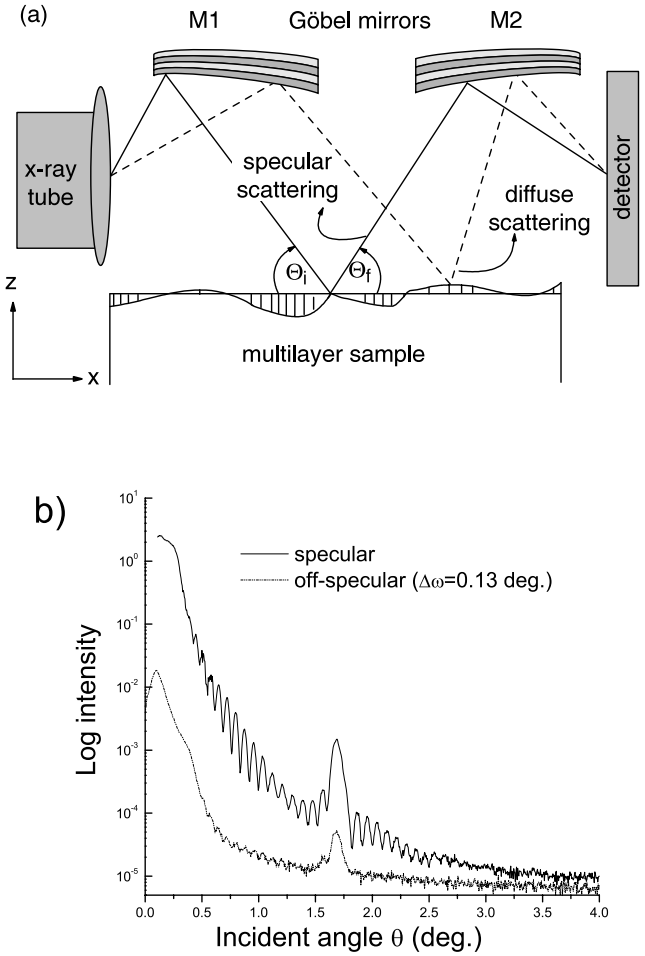

Figure 1. (a) Scattering geometry with grazing incidence and exit angles. M1 and M2 are Göbel mirrors which yield an enhanced intensity and suppress the $K\beta$ radiation. (b) Specular and off-specular scans of a Co/Cu ML from the S1 series: SiO_2/Co(1.45 nm)/[Cu(1.02 nm)/Co(1.45 nm)]$_{\times 20}$ with a Cu layer thickness corresponding to the first AF maximum.

vector (q_x, q_y) and contains information about the details of the lateral ordering of the interface roughness as well as the character of vertical replication of the roughness of subsequent interfaces. The strong interference effects occurring during the scattering of x-rays from an ML structure due to cumulative roughness replication and the dynamic nature of multiple x-ray scattering within an ML give rise to specific patterns of the diffuse intensity, that contain unique information on the nature of the interfacial structure. The recorded diffuse intensity can be used to determine the mesoscopic in-plane structure of surfaces and interfaces, the lateral correlation of roughness and the fractal dimension of jagged surfaces. For an ML structure, the intensity is weaker in the absence of vertical correlation, as there will be random phase relations between waves scattered from different layers. But there may be lateral correlations of roughness for each interface which result in diffuse scattering with well defined intensity distribution in the (q_x, q_y) plane, i.e. a weak dependence of the specular patterns on the lateral

interfacial parameters may be present in the second-order distorted-wave Born approximation (DWBA) [8]. The components of q along the in-plane and perpendicular directions can be expressed as $q_x = \frac{2\pi}{\lambda}(\cos\theta_f - \cos\theta_i)$ and $q_z = \frac{2\pi}{\lambda}(\sin\theta_f + \sin\theta_i)$, where λ is the x-ray wavelength, and θ_i and θ_f are the incident and exit angles with respect to the film surface (figure 1(a)). Therefore, the longitudinal scans of the diffuse scattering provide information about the roughness correlation of subsequent interfaces, while transverse scans (rocking curves) are sensitive to the height–height correlation function and thus the lateral coherence length of the interface roughness [25].

3.1.1. X-ray reflectivity (XRR). Figure 1(b) shows the specular reflectivity as well as the off-specular reflectivity of a sample from the S1 series with $N = 20$. The Bragg peak due to the periodicity of the ML is clearly visible in the specular reflectivity spectrum at about 1.7°, which agrees very well with the designated periodicity. The off-specular reflectivity replicates some of the features of the specular reflectivity. The presence of Bragg peaks and total thickness oscillations (Kiessig fringes) in the off-specular reflectivity signifies a high degree of vertical correlation of the interface structure from layer to layer with a vertical correlation length larger than the total thickness of the ML [26]. Thus, the spatial roughness pattern in successive layers is replicated from the substrate upwards to the top layers.

Using the coherent scattering approximation developed by Parratt [27] in 1954, a detailed analysis of the specular reflectivity pattern from a multilayered system can be done to obtain valuable information about the electron density in various layers and the width of its transitions at the interfaces. The latter is usually expressed in terms of an rms roughness σ. After subtraction of the off-specular reflectivity from the specular one, the true specular patterns are fitted by the least squares method using the standard optical formalism according to Nevot and Croce [28] with the following constraints.

(i) The roughness of the Co/Cu interfaces is allowed to evolve with increasing N. In order to keep the number of fit parameters controllable we introduce a new rms roughness parameter for each increment of N, e.g. from N_n to N_{n+1}, that describes the average roughness of the additional N_{n+1}–N_n bilayers. Only this new roughness parameter—we call it *evolving rms roughness* σ—is fitted, while all others are fixed at the value obtained from corresponding samples with smaller N. In this way we derive a true picture of changing interface roughness as N is varied.
(ii) The electron density and hence the refractive index of Co and Cu layers are taken to be smaller than the bulk value by about 1%, because generally in as-deposited, polycrystalline films the electron density is less than that in the bulk due to a higher density of imperfections.
(iii) The individual layer thicknesses are fitting parameters.
(iv) The top Co layer is expected to be oxidized, and hence its electron density as well as its thickness are separate fitting parameters.

Figure 2 shows true specular XRR patterns along with their fits for S1 and S2 type samples and representative values $N = 5$, 10 and 20. The fitted curves are shown by open symbols. We have not considered an interdiffused CoCu layer as negligible intermixing is expected for two elements (Co and Cu) with a positive heat of mixing. The thicknesses of the individual Co and Cu layers and the evolving σ values of each ML are determined from these fits. The σ values are listed in table 2 and plotted in figure 7(b) as a function of N. The error bars resulting from the fitting are rather small, indicating the adequacy of the model for our MLs. σ decreases when N increases for all three series S1, S2 and S3. This decrease is most prominent for S1, while for the S2 and S3 series due to an increased Cu layer thickness the changes are less

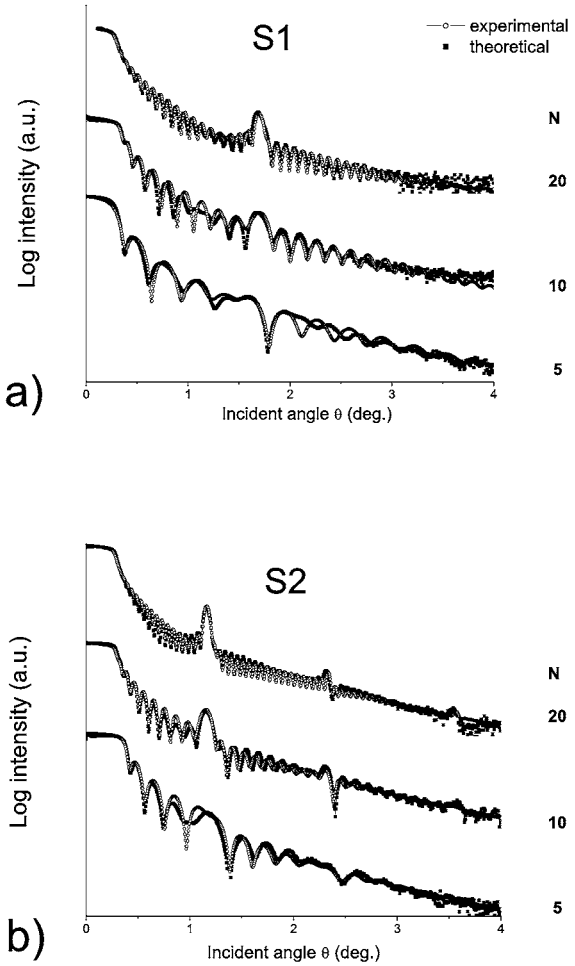

Figure 2. True specular scans of the MLs (a) SiO_2/Co(1.45 nm)/[Cu(1.02 nm)/Co(1.45 nm)]$_{\times N}$ (S1 series) and (b) SiO_2/Co(1.45 nm)/[Cu(2.20 nm)/Co(1.45 nm)]$_{\times N}$ (S2 series) along with fits for $N = 5$, 10 and 20. The curves are vertically shifted for clarity. The fitted evolving rms roughnesses σ are given in table 2.

significant. This result is in contradiction to the observation of Fulthorpe *et al* [29] who did not observe a change of the averaged interface roughness for a variation of N from 1 to 16. We suspect the poor quality of the MLs, which did not show interlayer coupling, as the cause for the absence of a systematic roughness variation in [29]. As seen in figure 7(b), σ decreases from S1 to S3 when the Cu spacer thickness increases. For the S1 series σ reaches—in particular for small N—values comparable to the Cu thickness, and we have to expect pinholes and magnetic bridging. For S2 and S3, σ corresponds to only about 40 and 25% of the Cu thickness.

In addition to the well defined Bragg peaks for $N = 10$ and 20 the presence of well defined finite thickness oscillations (Kiessig fringes) clearly indicates a well ordered layered structure irrespective of the variation of Λ. The quality of the data in terms of these resolved structures is comparable to or even better than the data reported from synchrotron radiation measurements using absorption edge contrast enhancement [16, 29]. We ascribe the good data quality to the usage of Göbel mirrors and take it as a further indication for the good structure of our MLs.

Table 2. Parameters obtained from the fitting of x-ray specular and diffuse scans. N is the number of bilayers for the S1 and S2 series corresponding to Cu thicknesses around the first and second AF maxima of the oscillatory interlayer coupling. The h parameter is 0.5 ± 0.2 for all simulations.

Series	N	Evolving rms roughness σ (nm)	Long and short wavelength lateral correlation lengths ξ and ξ' (nm)
S1	20	0.58 ± 0.01	$\xi = 10 \pm 10$; $\xi' = 5 \pm 5$
	10	0.65 ± 0.01	$\xi = 10$; $\xi' = 5$
	5	0.78 ± 0.02	$\xi = 10$; $\xi' = 5$
	3	1.1 ± 0.03	—
S2	20	0.54 ± 0.01	$\xi = 100 \pm 30$; $\xi' = 20 \pm 10$
	10	0.59 ± 0.02	$\xi = 50$; $\xi' = 20$
	5	0.64 ± 0.03	$\xi = 50$; $\xi' = 20$
	3	0.9 ± 0.03	—

For the S2 series the second order Bragg peaks are clearly resolved, whereas for the S1 series they are not visible. This is a further indication that the specimens of series S2 have a better layer structure and smoother interfaces than S1 samples. Finally, for $N = 5$ we cannot identify a Bragg peak for either S1 or S2 type samples (figure 2) because of a worse layer structure due to the increased rms roughness for smaller N.

Interface roughness is often assumed to scale with the number of bilayers when the two elements are almost indistinguishable. But if the roughness depends on interdiffusion or chemical reactions, then the interfacial roughness depends on the bilayer period Λ, too. The evolution of the morphologies of the individual layers, e.g. grain sizes, is more prominent for smaller individual layer thicknesses. Thus, short bilayer periods Λ have an enhanced influence on roughness. This is, for instance, why short period x-ray mirrors are found to be inefficient reflectors [30]. In the present case, as the bilayer periods are of the same order of magnitude as the grain sizes, we expect N to have a clear influence on the roughness. The evolution of roughness σ with the total ML thickness t can be described by the law [31]

$$\sigma \propto t^{\beta}, \tag{1}$$

where β is the growth exponent. In the double-logarithmic plot of σ versus the total ML thickness t in figure 3 the β values can be deduced from the slopes. The slopes for series S1 and S2 are almost the same, $\beta \approx -0.15 \pm 0.02$. The effect of the Cu thickness on β is more pronounced for lower total ML thicknesses (lower N), because the plots for S1 and S2 tend to coincide for $N > 20$. This may be attributed to a saturating behaviour of σ with increasing number of interfaces.

3.1.2. X-ray diffuse scattering (XDS). Diffuse scattering measurements provide information about the structure of the interfaces in the plane of the film, which can be described in terms of a height–height correlation function $C_0(x, y)$. In most cases it is written as [24]

$$C_0(x, y) = \sigma^2 \exp\left(-\left[\frac{|R|}{\xi}\right]^{2h}\right), \tag{2}$$

where $R = (x^2 + y^2)^{1/2}$, and ξ is the in-plane correlation length of the interface height variations. The parameter h is the fractal dimension of the relief and describes the jaggedness of the interface [13].

Several basic models for the roughness cross correlation within an ML have been reported in the literature. The models are developed based on the different possibilities of roughness

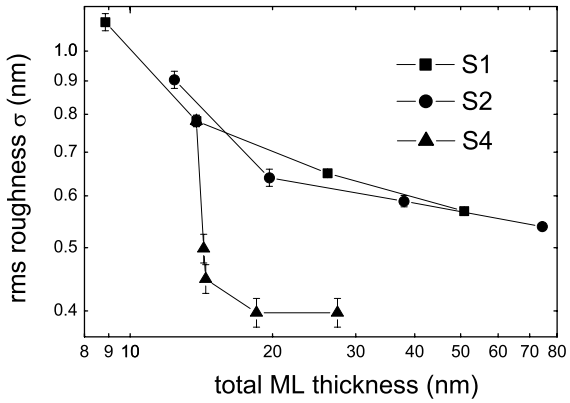

Figure 3. Double logarithmic plot of σ versus the total ML thickness t for series S1, S2 and S4. The growth exponent β is estimated from the slope of the curves.

correlation along the ML structure. In our study we have tried three different models of vertical and lateral roughness correlations according to the models in [26, 32], and [33]: the model of Holý and Baumbach [26] assumes complete correlation. It takes into account that interfaces are formed successively from the substrate to the surface. Each interface adds some statistically independent roughness, which is assumed to be completely transferred to all subsequent interfaces. Thus, the roughness is accumulated. The correlation between any two interfaces i and j is determined by the contributions of all the interfaces below because the roughness added between i and j is independent of the roughness of the lower interface i. The rms roughness of this model always increases with N. The model of Spiller *et al* [32] also assumes accumulation of roughness as in the model of Holý and Baumbach, but the roughness added at each interface is not completely inherited by subsequent interfaces. The degree of inheritance is lower for shorter lateral wavelengths of the roughness. As a result, the lateral wavelength of the total roughness grows towards the surface, even if all interfaces add roughness with the same lateral wavelength. The total rms roughness may increase or decrease towards the surface depending on whether the accumulation of short wavelengths or dissociation of long wavelengths is dominant. The model of Ming *et al* [33], finally, describes the intermediate case between uncorrelated roughness—each interface is assumed to possess a fractal (self-affine) roughness with the correlation function $C_0(x, y)$ (equation (2)) as given by Sinha *et al* [24]—and completely correlated roughness. In this model the vertical correlation does not depend on the lateral wavelength of the roughness. The replication factor is solely controlled by a vertical correlation length κ and the full correlation function is given by

$$C_z(x, y) = C_0(x, y) \exp\left(-\left[\frac{|z|}{\kappa}\right]\right), \tag{3}$$

where $C_0(x, y)$ is the height–height correlation (or self-correlation) function of a single interface and z the vertical coordinate measuring the distance between interfaces. The vertical correlation length κ can vary from zero (no correlation) to much larger than the thickness of the ML (high correlation).

We could not find parameter sets to bring the simulated and measured profiles into agreement for a set of samples either for the model of Holý and Baumbach or for that of Spiller *et al*. Good agreement can only be achieved with the model of Ming *et al*, for which the information from in-plane and out-of-plane correlation is decoupled. This may be due to the fact that the replication of the roughness across layers is neither incremental

nor accumulative, but of 'restarting-layer' type [20]. Restarting behaviour may occur due to different chemisorption at Co/Cu and Cu/Co interfaces. It has been observed for non-magnetic Si/Mo [20] and Pt/C [12] MLs. Therefore, we fitted the non-specular data using the program TRDS-sl [36] according to the model of Ming *et al* [33]. Figure 4 shows the XDS patterns of S1 and S2 specimens with various N for two different scattering angles (i.e. q_z) corresponding to the first and second order Bragg peaks.

For larger q_x (i.e. $\omega-\theta$), the transverse scan is more sensitive to short wavelength waviness of the interfacial roughness according to $\xi = 2\pi/q_x$ [34]. The smaller the scattering angle θ (i.e. the lower the Bragg order), the more we are geometrically blocked from measuring scattered intensity due to small wavelength roughness because ω must be smaller than θ. The shortest correlation length is given by $\xi_{limit} = 2\pi/q_{x^{max}}$ (about 80 and 20 nm for the first and second order Bragg peaks of the S1 series; 175 and 45 nm for the S2 series). Nevertheless, roughness with a wavelength smaller than ξ_{limit} still has an influence on the scattered x-ray intensity within the accessible momentum window $|q_x| \leqslant |q_{x^{max}}|$. As shown by Savage *et al* [11, 35], this influence on the scattered intensity can still be fitted, and the fitting is fine and yields meaningful results as long as most of the scattered intensity is within the accessible window.

The fitting variables are the lateral correlation lengths ξ and ξ' from the first and second order Bragg peaks respectively, and the fractal dimension h. The vertical correlation length κ is found to be larger than the total ML thickness. The long and short wavelength correlation lengths for S1 and S2 specimens along with their typical uncertainties are given in table 2. The amplitude of the short wavelength (ξ') correlations is much smaller compared to the amplitude of the long wavelength (ξ) correlations, and their effect on the multilayer can thus be neglected. The variations of ξ with N for the S1 and S2 series are within the error bars in agreement with recent observations of Santamaria *et al* [37] in Fe/Cr MLs grown by magnetron sputtering. These authors found an increase of the roughness with N, similar to Schmidt *et al* [7] for epitaxial Fe/Cr MLs grown by molecular beam epitaxy. In the present study, however, we observe a *decrease* of σ with increasing N from specular scattering data. The lateral correlation for the S2 series ($\xi \approx 50$ nm) clearly exceeds the value of the S1 series ($\xi \approx 10$ nm), while the jaggedness of the interfaces shows no significant difference. The roughness of an ML structure does not necessarily scale with the total thickness in a similar fashion as the roughness of a single film. Whereas some MLs show an increase in roughness with N [4], some others can 'heal' the roughness[38] depending on thermodynamic quantities and the lateral wavelength of the roughness.

The increase of ξ for S2 is a signature of the influence of the individual layer thickness on the lateral correlation of roughness in the ML. In figure 7(b) σ converges to a minimum for all three series, but it is reached faster for series S2 and S3 at about $N = 10$ compared to $N > 20$ for S1. The Cu layer thickness is believed to modify the growth and thereby the roughness evolution. Co/Cu is a system with positive heat of mixing. The resulting high surface mobility may foster island formation and can result in poor layering with a short lateral correlation length ($\xi \approx 10$ nm for S1). An increase of the Cu thickness and thus also t increases ξ according $\xi \propto t^{\alpha}$ [31] with a scaling exponent $\alpha \approx 0.76$, which characterizes self-affine surface roughness [13]. From the comparison of $\alpha \approx 0.76$ with $\beta \approx -0.15$ for series S1 and S2 it follows that the fast increase of ξ is dominantly responsible for the smoothening of the layers [39]. The translation of growth exponents to dynamic scaling factors is based on the assumption that the deposition rate is constant throughout the growth of the ML, and the saturation time is translated into the thickness of the vertically correlated ML. The value of ξ typically characterizes the lateral sizes of 'domed columns' [40] characteristic of zone 1 in Thornton's classification scheme [41]. Zone 1 is typical for sputtered films for which the melting temperature of the deposited material is higher than the substrate temperature.

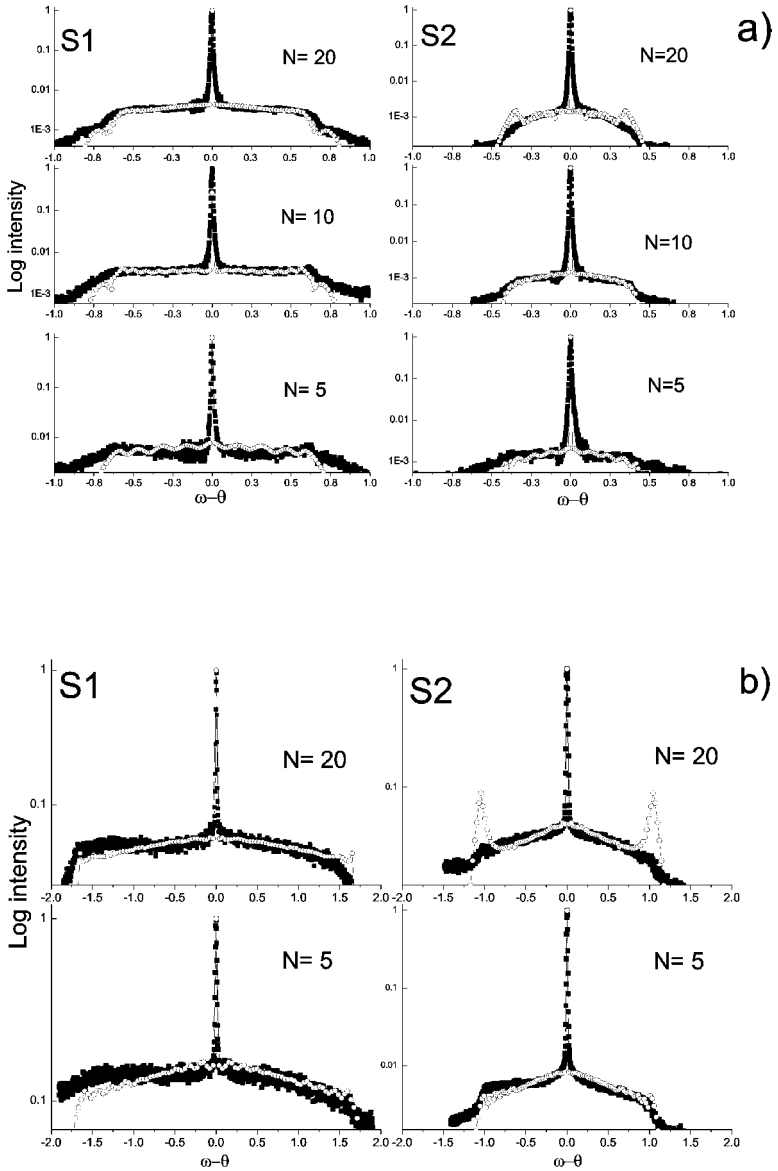

Figure 4. Transverse rocking scans of the MLs SiO_2/Co(1.45 nm)/[Cu(1.02nm)/Co(1.45nm)]$_{\times N}$ (S1 series) and SiO_2/Co(1.45 nm)/[Cu(2.20nm)/Co(1.45nm)]$_{\times N}$ (S2 series) along with their fits at the scattering angle around (a) the first Bragg peak for $N = 5$, 10 and 20 and (b) the second Bragg peak for $N = 5$ and 20 (the diffuse streaks at $|\omega - \theta|$ equal to the second order Bragg angle for the S2 series with large N are beyond the instrumental resolution). The lateral correlation lengths along with the fractal dimension h extracted from the fits are given in table 2.

In our case, the substrate temperature is RT and is not expected to increase due to very low sputtering rates.

3.1.3. Atomic force microscopy (AFM). AFM micrographs (in figure 5 we display examples of the S1 and S2 series for $N = 20$) of the S2 series show large 'clusters' or signatures of

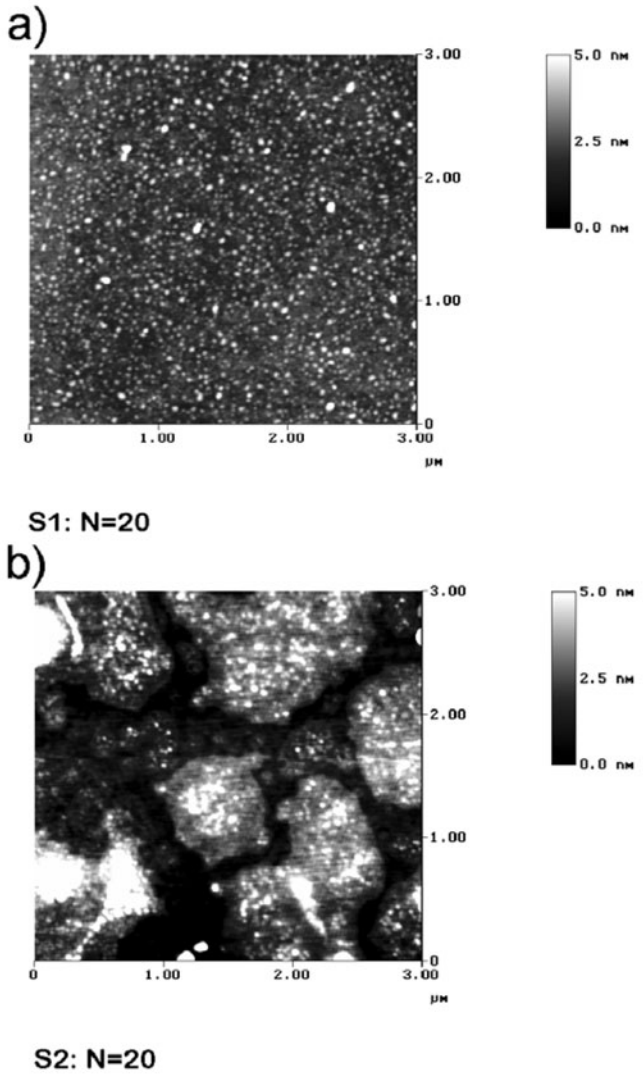

Figure 5. AFM micrographs of the MLs (a) SiO_2/Co(1.45 nm)/[Cu(1.02 nm)/Co(1.45 nm)]$_{\times 20}$ (S1 series) and (b) SiO_2/Co(1.45 nm)/[Cu(2.20 nm)/Co(1.45 nm)]$_{\times 20}$ (S2 series) corresponding to the first and second AF coupling maxima, respectively. Image size: 3 μm $\times$ 3 μm.

'domed columns' of individual grains with sizes of the order of 1.0 μm, whereas for the S1 series no such 'clusters' are observable. These images reveal a significant difference for the S1 and S2 series. The average size of the individual grains in the images is $\approx 70 \pm 10$ nm in both cases and is also similar for different N. Thus, the long wavelength correlation length ξ as measured by XDS is roughly determined by the grain size [19]. Quantitative variances between AFM and XDS with a larger grain size determined by AFM may arise from (i) the surface versus bulk sensitivity, (ii) tip shape effects in AFM and (iii) oxidation of the surface upon air exposure. Nevertheless, the AFM images show that the larger Cu layer thickness of the S2 series induces the formation of cluster-like structures (figure 5(b)) on a length-scale which is much larger than the grain size and beyond the resolution limit of our XDS spectra.

3.2. Magnetic characterization: MOKE and magnetotransport

Figure 6 shows the MOKE hysteresis loops for S1, S2 and S3 specimens with varying N. The ratio of magnetic remanence M_r and the magnetic saturation M_s can be used to quantify the fraction of an ML with antiparallel alignment of adjacent film magnetizations at zero external field. This so-called antiferromagnetic coupling fraction (AFF) is given by [42]

$$\mathrm{AFF} = 1 - \frac{M_r}{M_s}. \tag{4}$$

The GMR ratio of an ML scales with the AFF because only AF coupled regions of a sample can contribute to the magnetoresistance. From the data in figure 6 we obtain an increase of the AFF with increasing N for the series S1 and S2, while for the S3 samples FM coupling dominates, making the AFF small and rather constant with N (see figure 9(a)). In the S1 and S2 series, we find the Co layers decoupled (or FM coupled) for $N \leqslant 3$, whereas AF coupling dominates for $N > 3$. This can be understood considering the enhanced roughness for small N, which can give rise to magnetic bridges across the Cu layers as mentioned above. These MOKE results are also verified by SQUID data.

In figure 7(a) we plot the electrical resistance in the magnetically saturated state, the saturation resistance R_s, of the MLs as a function of N. R_s is expected to drop inversely proportional with increasing total ML thickness. Therefore, R_s of the S1 series is shown versus $1/N$ in the inset. The slope is not constant but slightly increasing. This indicates an enhanced contribution from interface resistances below $N = 10$ in agreement with the enhanced interface roughness σ (figure 7(b)).

We define the GMR ratio the usual way by $(R_0 - R_s)/R_s$, where R_0 is the maximum resistance near zero field. In figure 8 we present magnetoresistance curves of sample series S1 and S2 for various N. The field axes are the same for each series with the exception of $N = 3$ in figure 8(a). In figure 9 we plot the AFF in direct comparison with the GMR ratio. For series S1, the GMR curve becomes flatter for $N > 10$ and reaches a maximum value of 46%. The data for the S2 series behave similarly, but the GMR ratio does not exceed 20%. The larger ξ of series S2 inferred from x-ray measurements may be the reason for larger AFF and GMR around $N = 5$ compared to series S1. It has been reported that thin Cu layers ($\leqslant$1.0 nm) may give inconsistent results mainly because of incomplete layering [43] causing magnetic bridging through pinholes [44]. This is not the case for our samples when N is big enough, because we observe high GMR values and oscillatory coupling with a period of about 1.0 nm Cu thickness.

The steep increase of the GMR ratio with N is clearly correlated with the trend of the AFF. For the S2 series the rise of the AFF as well as the GMR ratio starts for a lower value of N, and the increase is more gradual than for the S1 series. For the S3 samples the GMR ratio as well as the AFF are fairly unaffected by changing N. Obviously, the GMR ratio does not have a linear relationship to N; it is rather largely dependent on the growth morphology as indicated by the different slopes of the GMR versus N curves in figure 9(b). The difference is most obvious for S1 compared to that of S2 and S3. This indicates that the contribution from interface scattering starts to play a significant role only for $N > 10$. This is most prominent for S1 due to the larger interface to bulk scattering ratio at smaller spacer thickness.

In order to combine the observations of x-ray scattering and MOKE with the GMR data, we visualize the growth mechanism of the MLs for increasing N in a scheme in figure 10. We observe a low GMR ratio below $N = 5$ for the series S1. This is not unexpected in view of the high rms interface roughness reaching values comparable to t_{Cu} in combination with the small lateral correlation length (grain size) of only $\xi = 10$ nm. We expect that most of the layers are discontinuous and thus form an intermixed layer. Therefore, the small

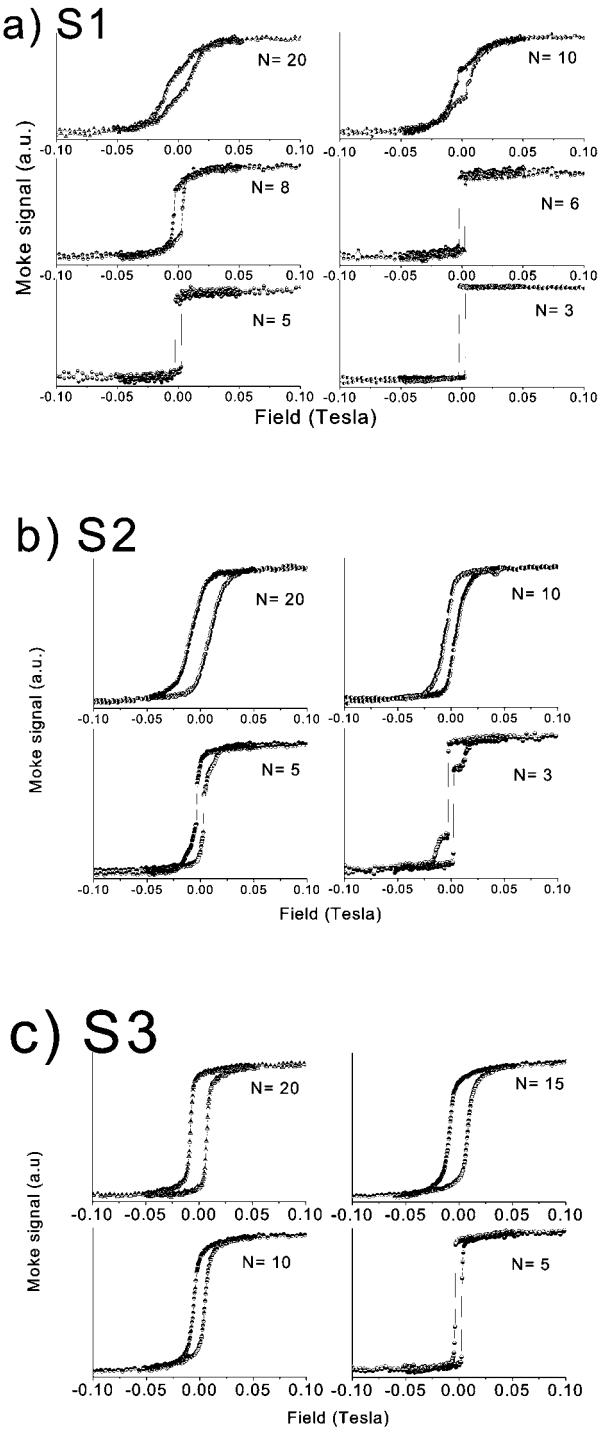

Figure 6. MOKE hysteresis loops for the MLs (a) SiO_2/Co(1.45 nm)/[Cu(1.02 nm) /Co(1.45 nm)]$_{\times N}$ (S1 series), (b) SiO_2/Co(1.45 nm)/[Cu(2.20nm)/Co(1.45nm)]$_{\times N}$ (S2 series) and (c) SiO_2/Co(1.45 nm)/[Cu(2.50nm)/Co(1.45nm)]$_{\times N}$ (S3 series) for various N.

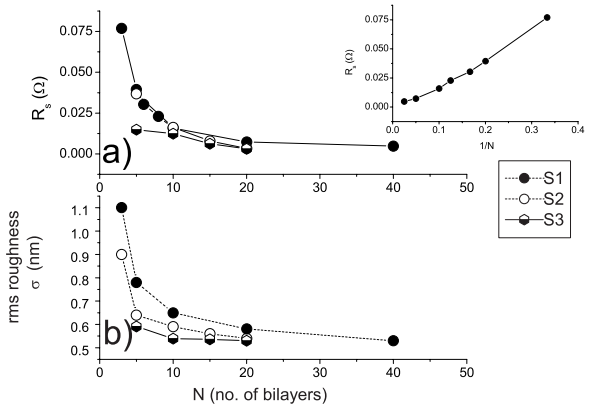

Figure 7. (a) Saturation resistance R_s and (b) evolving rms interface roughness σ as a function of N for samples series S1, S2 and S3. The inset in (a) shows R_s of series S1 versus $1/N$.

increase of the AFF and the GMR ratio below $N = 5$ is attributed mainly to scattering from magnetic sites in the bulk of this intermixed layer, similar to the situation in granular Co/Cu systems [45]. This similarity is supported by the triangular shape and the high field wings of the magnetoresistance curve in figure 8(a) for $N = 3$: typical features of granular systems. For $N > 5$ the layering improves such that the topmost layers become continuous as indicated by the reduced evolving rms roughness. In this range AF coupling sets in. Around $N = 10$, there is the maximum increase of the AFF due to the formation of a completely layered structure in consistency with the flattening of the σ curve (figure 7(b)). Beyond $N = 10$, where the AFF saturates, the small increase of the GMR ratio is attributed to a further improvement of the average interface quality because σ still slightly decreases in this region (figure 7(b)). The first few bilayers at the bottom always remain badly ordered and serve merely as a buffer for the upper, well ordered bilayers, which give rise to the high GMR ratios.

For the S2 series the AFF increases at smaller N due to the smaller rms roughness (less than 40% of t_{Cu}) and the correlation length ξ is five times larger than for S1. The formation of continuous layers sets in earlier and more gradually. Hence, the rise of the GMR ratio is also more gradual. The lower ξ of series S1 is likely to be the reason for the lower AFF below $N = 5$, as so-called 'orange peel coupling' may set in, which reduces the AF interlayer exchange coupling for conformal ML [46]. A scheme in figure 11 shows the influence of ξ on the orange peel coupling for S1 and S2, respectively. Free magnetic poles arising due to topological roughness (plus and minus signs in figure 11) cause a stray field in the spacer layer. For conformal interface roughness, flux closure is achieved when adjacent layers are parallel magnetized. Therefore, conformal roughness results in FM interlayer coupling. Its strength depends on the number of free poles and thus on ξ. For higher N, however, the interface roughness decreases, and the AF exchange coupling becomes the dominant contribution. The smaller GMR magnitude of the S2 series for $N > 5$ is related to its smaller AFF. In the second AF maximum the coupling is weaker, such that inhomogeneities, as for instance roughness, have a stronger impact and reduce the AFF. However, the influence of the correlation length for conformal AF coupled ML is more effective at lower N.

4. Variation of the bottom-most Co thickness

From the above results and discussions one may arrive at the conclusion that a single layer with a thickness equivalent to about five Co/Cu bilayers, i.e. $[1.45\,\text{nm Co}/1.02\,\text{nm Cu}]_{\times 5} = 12.35$ nm,

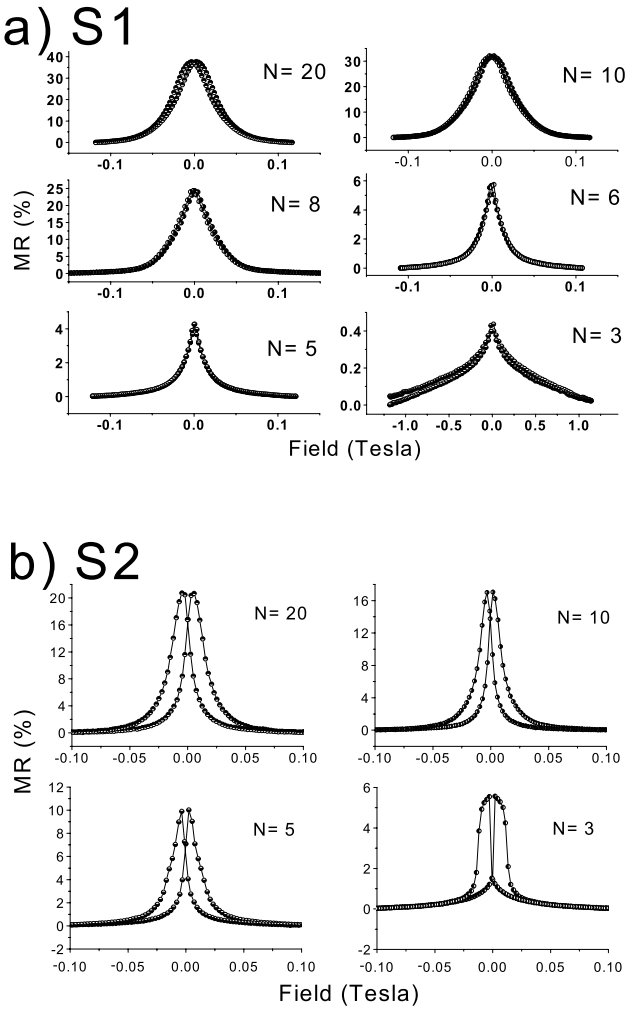

Figure 8. The magnetoresistance curves for MLs (a) SiO_2/Co(1.45 nm)/[Cu(1.02 nm) /Co(1.45 nm)]$_{\times N}$ (S1 series) and (b) SiO_2/Co(1.45 nm)/[Cu(2.20 nm)/Co(1.45 nm)]$_{\times N}$ (S2 series) for various N. Note in (a) the different field axis for $N = 3$.

may be necessary to obtain good growth of continuous of Co and Cu layers. We test this idea by depositing the bottom-most Co layer with different thicknesses t_{Co} prior to the deposition of the ML (see table 1). This series of MLs (labelled S4) is prepared using the same parameters as for the sample of series S1 with $N = 5$. Possibly, this procedure allows us to reduce the number of bilayers in an ML without a reduction of the GMR ratio.

Figure 12 shows the variation in the true specular x-ray patterns along with the fits for increasing layer thickness of the bottom-most Co layer t_{Co}. The spectra are fitted in a similar way as described above except that the roughness is described by a single parameter, the average rms roughness $\overline{\sigma}$. We kept all the fitting parameters obtained from the S1 sample with $N = 5$ constant, while we fitted only t_{Co} and $\overline{\sigma}$ as indicated in the figure for five representative samples of series S4. $\overline{\sigma}$ monotonically decreases from 0.8 nm at $t_{\mathrm{Co}} = 1.45$ nm to 0.4 nm at $t_{\mathrm{Co}} = 15.1$ nm. The changes in the lateral correlation lengths ξ estimated from XDS spectra are within the error bars of the measurements.

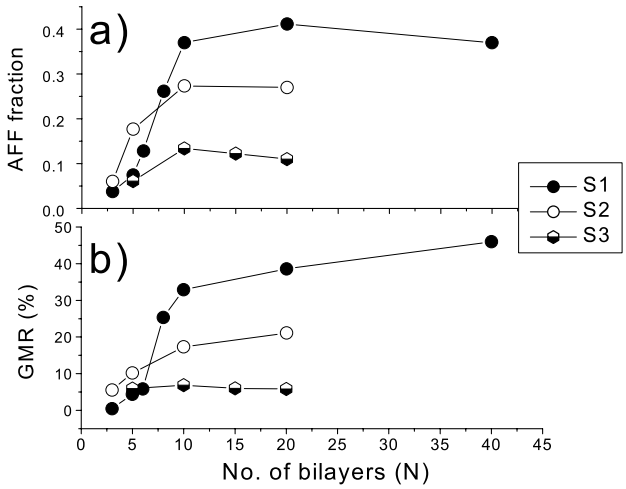

Figure 9. (a) AFF and (b) GMR ratio as a function of N for samples series S1, S2 and S3.

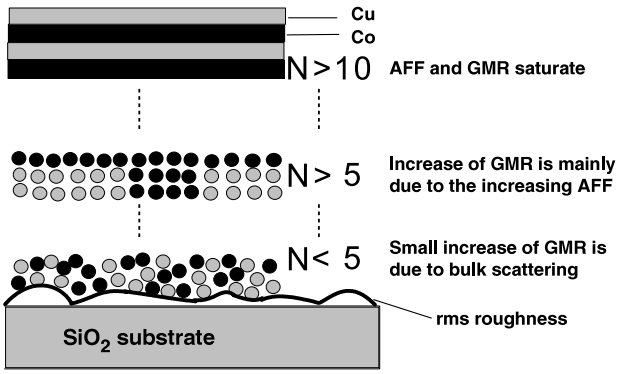

Figure 10. Scheme of the layered structure with three qualitatively different regions along the vertical position in the ML stack. Each region contributes differently to the GMR ratio of the whole structure.

The growth exponent β in figure 3 shows a clearly larger value for series S4 compared to the S1 and S2 series. In fact, for series S4 there are two different slopes and hence two different growth exponents. For $t_{Co} < 2.0$ nm, β is ≈ -10.0 and is therefore of much more significance than $\beta \approx -0.15$ for the previously discussed ML series S1 and S2. But beyond this thickness, β attains a similar value as for series S1 and S2. Modifying the Co layer thickness t_{Co} by only a few ångströms considerably increases β, unlike the changes from series S1 to S3 where we have modified the Cu layer thickness (see the XDS section). Different roughness evolutions for single Cu and Co layers may be responsible for this behaviour. The different β values can also be seen as support for the 'restarting-type' model of growth. The evolution of the ML roughness (the smoothening) is disturbed as each new layer is grown on the outer surface of the previous layer with different thermodynamic properties, e.g. different melting points. Of course, this is not the case for a single-layer film of similar thickness. Thus, there is no change in ξ for S4.

The result of our test is shown in figure 13, where we plot the AFF (filled and open squares, left-hand axis) and the GMR ratio (filled circles, right-hand axis) as a function of t_{Co}.

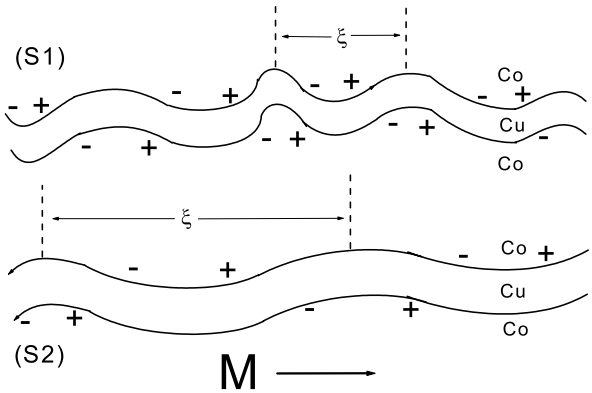

Figure 11. Schematic representation of the influence of ξ on the 'orange peel' coupling for series S1 and S2. Plus and minus signs represent magnetic charges to visualize the roughness-induced stray fields that give rise to a FM coupling contribution.

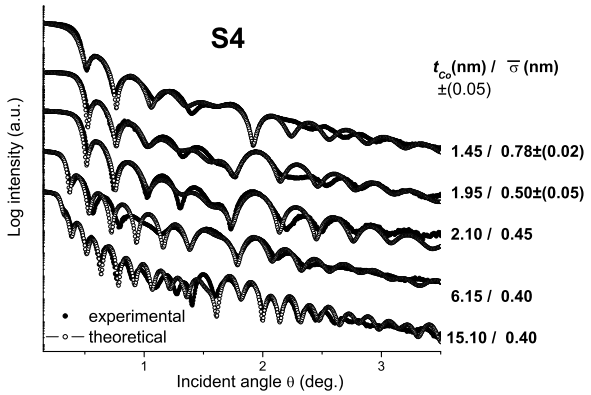

Figure 12. True specular XRR scans of the MLs $SiO_2/t_{Co}/[Cu(1.02\ nm)/Co(1.45\ nm)]_{\times 5}$ of series S4 with different bottom Co layer thicknesses t_{Co} along with fits. The fitted averaged rms roughnesses $\overline{\sigma}$ are listed.

The AFF given by open squares is determined according to equation (4) without considering the contribution of the bottom-most Co layer to the saturation and remanent magnetization of the whole stack. For the filled squares the magnetization M_b of the bottom-most Co layer exceeding the thickness 1.45 nm is fully taken into account when calculating the AFF,

$$\mathrm{AFF} = 1 - \frac{M_r - M_b}{M_s - M_b}, \tag{5}$$

where M_r and M_s denote the remanent and saturation magnetizations of the whole stack, respectively. This correction has little effect for small t_{Co}, but enhances the AFF by more than a factor of two for $t_{Co} = 15.1$ nm. The AFFs derived from MOKE data are smaller than the filled squares due to the finite penetration depth of the light, but definitely larger than the open squares. Both GMR ratio and AFF show similar features: (i) an increasing background and (ii) a sharp peak around $t_{Co} = 2.0$ nm. Note that the GMR ratio reaches values of up to $\approx$20%.

The increasing background which shows an enhancement of the GMR ratio from 4.5% at $t_{Co} = 1.45$ nm to 13.5% at $t_{Co} = 15.1$ nm is the qualitative result that we expect based on the previous section: a thicker bottom Co layer improves the sample structure leading to an

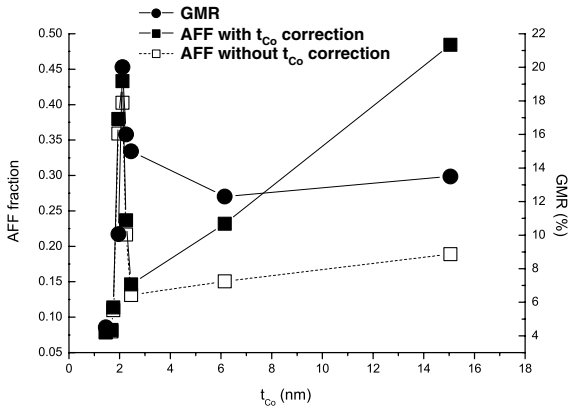

Figure 13. AFF (filled and open squares, left-hand axis) with and without correction for the remanent magnetization of the bottom-most Co layer and corresponding GMR ratios (filled circles, right-hand axis) as a function of the thicknesses of the bottom-most Co layer (t_{Co}) for the ML $SiO_2/t_{Co}/[Cu(1.02\ nm)/Co(1.45\ nm)]_{\times 5}$ (S4 series).

enhancement of the AFF, which, in its turn, results in a higher GMR ratio. Quantitatively, we note that the GMR ratio is only half as large compared to the series S1, although the AFF is similar (figure 9). For instance, we find a GMR ratio of 34% for the S1 sample with $N = 10$ and only 14% for the S4 sample with $t_{Co} = 15.1$ nm, although the AFF of the S4 sample is likely to be comparable to the 0.37 of the S1 sample. Therefore, the intrinsic GMR (i.e. the GMR ratio divided by the AFF) is larger for the S1 series. This can easily be explained by taking into account that the bottom-most Co layer acts as a shunting resistor in parallel connection to the Co/Cu bilayers that give rise to the GMR effect.

AFM micrographs of series S4 reveal a decrease of the average grain sizes with increasing t_{Co} from 70 ± 10 nm for $t_{Co} = 2.10$ nm to 30 ± 10 nm for $t_{Co} = 15.1$ nm. Smaller grains not only cause a decrease in the rms roughness but also result in a reduced intergrain exchange coupling and thereby increase the AFF. Thus, the larger AFF and enhanced spin-dependent grain boundary scattering contribute to the increase of the GMR ratio, while the role of the interface roughness is negligible here.

The occurrence of sharp peak at $t_{Co} = 2.0$ nm is surprising because it is caused by only a small variation of the thickness of one layer by a few ångström in an ML that consists of ten layers in total. We find the qualitatively same behaviour for a second, independently prepared sample series of the type S4. The origin of the sharp peak around $t_{Co} = 2.0$ nm is not understood and requires further investigations, e.g. with samples where the thickness of other Co layers in the ML is varied. Such studies are under way.

5. Conclusions

High quality Co/Cu MLs grown by dc magnetron sputtering show a high degree of correlation along the growth direction and small interface roughness, but a significant dependence of the roughness on the number of bilayers N. These changes in growth morphology due to increasing N and their influence on magnetic properties and magnetotransport have been studied in detail.

The results give insight into the growth dynamics, particularly in the evolution of interface roughness along Co/Cu MLs. The evolving rms roughness σ decreases with N, and the growth exponent of the roughness (β) is found to be influenced by the presence of interfaces and the

thickness of individual layers. The lateral correlation length (ξ), however, does not vary with N, but is larger for a larger Cu spacer thickness corresponding to the second AF coupling maximum compared to the first AF coupling maximum.

The GMR ratio depends largely on the growth morphology as well as on the number of interfaces. The influence of the lateral correlation length for conformal and AF coupled MLs is bigger at lower N. The role of interface scattering becomes significant only for $N > 10$. The observed increase of the GMR ratio for $N > 5$ is mainly due to the enhancement of the AF coupling fraction AFF. GMR ratios up to 35% are reached for $N = 10$. We conclude that the first few ($\approx$5) bilayers act like a buffer system and enable the growth with sufficiently high layer quality for the subsequent bilayers. This idea of 'passive bilayers' at the bottom of the stack is confirmed by replacing the first few bilayers by a bottom-most Co layer of equivalent thickness. Surprisingly, the AFF and the GMR ratio sensitively depend on the thickness of this bottom-most Co layer and show a pronounced peak for $t_{\mathrm{Co}} = 2.0$ nm with a GMR ratio of 20% for $N = 5$. Further work is needed to unravel this observation.

Similarly subtle dependences of the magnetotransport on structure might play a role for sputtered MLs consisting of other materials than Co and Cu.

Acknowledgments

We thank U Rücker for his cooperation with the x-ray diffractometer. This work is supported by the HGF-Strategiefondsproject 'Magnetoelectronics'.

References

[1] Baibich M N, Broto J M, Fert A, Nguyen van Dau F, Petroff F, Etienne P, Creuzet G, Friedrich A and Chazelas J 1988 *Phys. Rev. Lett.* **61** 2472
[2] Parkin S S P, More N and Roche K P 1990 *Phys. Rev. Lett.* **64** 2304
[3] Fullerton E E, Conover M J, Mattson J E, Sowers C H and Bader S D 1993 *Appl. Phys. Lett.* **63** 1699
[4] Fullerton E E, Kelly D M, Guimpel J, Schuller I K and Bruynserade Y 1992 *Phys. Rev. Lett.* **68** 859
[5] Olligs D, Bürgler D E, Yang Y G, Kentzinger E, Rücker U, Schreiber R, Brückel Th and Grünberg P 2002 *Europhys. Lett.* **59** 458
[6] Gupta A, Paul A, Chaudhari S M and Phase D M 2000 *J. Phys. Soc. Japan* **69** 2182
[7] Schmidt C M, Bürgler D E, Schaller D M, Meisinger F, Güntherodt H-J and Temst K 2001 *J. Appl. Phys.* **89** 181
[8] Fullerton E E, Pearson J, Sawers C H, Bader S D, Wu X Z and Sinha S K 1993 *Phys. Rev.* B **48** 17432
[9] See articles in
Lagally M G (ed) 1990 *Kinetics of Ordering and Growth at Surfaces* (New York: Plenum)
[10] Salditt T, Metzger T H and Peisl J 1994 *Phys. Rev. Lett.* **73** 2228
[11] Savage D E, Kleiner J, Schimke N, Phang Y H, Jankowski T, Jacobs J, Kariotis R and Lagally M G 1991 *J. Appl. Phys.* **69** 1411
[12] Paul A and Lodha G S 2002 *Phys. Rev.* B **65** 245416
[13] Salditt T, Schimke N, Phang Y-H and Lagally M G 1992 *J. Appl. Phys.* **71** 3283
[14] Parkin S S P, Bhadra R and Roche K P 1991 *Phys. Rev. Lett.* **66** 2152
[15] Kano H, Kagawa K, Suzuki A, Okabe A, Hayashi K and Aso K 1993 *Appl. Phys. Lett.* **63** 2839
[16] Marrows C H, Wiser N, Hickey B J, Hase T P A and Tanner B K 1999 *J. Phys.: Condens. Matter* **11** 81
[17] Parkin S S P 1993 *Phys. Rev. Lett.* **71** 1641
[18] Chapman J N, Rose J, Aitchison P A, Holloway H and Kubinski D J 1999 *J. Appl. Phys.* **86** 1611
[19] Paul A 2002 *J. Magn. Magn. Mater.* **240** 497
[20] Freitag J M and Clemens B M 2001 *J. Appl. Phys.* **89** 1101
[21] Ueda H, Kitakami O, Shimada Y, Goto Y and Yamamoto M 1994 *Japan. J. Appl. Phys.* **33** 6173
[22] Saito Y, Inomata K, Yusu K, Goto A and Yasuoka H 1995 *Phys. Rev.* B **52** 6500
[23] Lucinski T, Reiss G and Brückl H 1999 *J. Magn. Magn. Mater.* **193** 484
[24] Sinha S K, Sirota E B, Garoff S and Stanley H B 1988 *Phys. Rev.* B **38** 2297

[25] de Boer D K G 1994 *Phys. Rev.* B **49** 5817
[26] Holý V and Baumbach T 1994 *Phys. Rev.* B **49** 10668
[27] Parratt L G 1954 *Phys. Rev.* **95** 359
[28] Nevot L and Croce P 1980 *Rev. Phys. Appl.* **15** 761
[29] Fulthorpe B D, Joyece D E, Hase T P A, Rozatian A S H, Tanner B K and Grundy P J 1999 *J. Phys.: Condens. Matter* **11** 8477
[30] Barbee T W Jr 1985 *SPIE* **2** 563
[31] Family F 1986 *J. Phys. A: Math. Gen.* **19** L441
[32] Spiller E, Stearns D and Krumrey M 1993 *J. Appl. Phys.* **74** 107
[33] Ming Z H, Krol A, Soo Y L, Kao Y H, Park J S and Wang K L 1993 *Phys. Rev.* B **47** 16373
[34] Phang Y-H, Savage D E, Kariotis R and Lagally M G 1993 *J. Appl. Phys.* **74** 3181
[35] Savage D E, Shimke N, Phang Y-H and Lagally M G 1992 *J. Appl. Phys.* **71** 3283
[36] Kindly provided by
Stepanov S, Illinois Institute of Technology, Chicago
[37] Santamaria J, Gomez M-E, Cyrille M-C, Leighton C, Krishnan K M and Schuller I K 2002 *Phys. Rev.* B **65** 12412
[38] Houdy Ph, Boher P, Schiller C, Barchewitz P, Alehyane N and Quahabi M 1988 *Proc. SPIE* **95** 984
[39] Paniago R, Forrest R, Chow P C, Moss S C, Parkin S S P and Cookson D 1977 *Phys. Rev.* B **56** 13442
[40] Kahanda G L M K S, Zou X, Farrell R and Wong P 1992 *Phys. Rev. Lett.* **68** 3741
[41] Thornton J A 1977 *Annu. Rev. Mater. Sci.* **7** 239
[42] Schad R, Beliën P, Verbanck G, Moshchalkov V V, Bruynseraede Y, Fischer H E, Lefebvre S and Bessiere M 1999 *Phys. Rev.* B **59** 1242
[43] Zhang H, Cochrane R W, Huai Y, Mao M, Bian X and Muir W B 1994 *J. Appl. Phys.* **75** 6534
[44] Hylton T L, Coffey K R, Parker M A and Howard J K 1993 *Science* **261** 1021
[45] Berkowitz A E, Mitchell J R, Carey M J, Young A P, Zhang S, Spada F E, Parker F T, Hutten A and Thomas G 1992 *Phys. Rev. Lett.* **68** 3745
[46] Chopra H D, Hockey B J, Chen P J, Egelhoff W F Jr, Wutting M and Hua S Z 1997 *Phys. Rev.* B **55** 8390